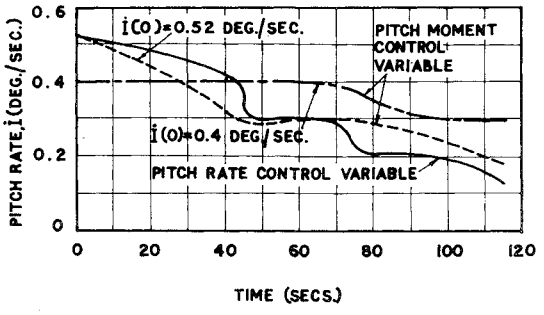

Fig. 2 Comparison of pitch-rate history with pitching moment and pitch rate as control variables.

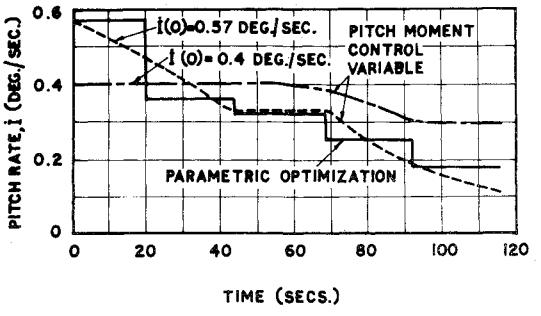

Fig. 3 Comparison of pitch-rate history with pitching moment and discretized pitch-rate as control variables.

comparisons are made with parametric optimization with discretized pitch-rates as parameters. Here, $\dot{i}$ (0) comes to be 0.57 deg/sec, instead of the given value of 0.4 deg/sec. This figure also shows that the pitch-rate control variable results differ significantly from the results of the present analysis.

The final altitude in all the above cases is the same (400 km) to an accuracy of 0.01 km. The injection is horizontal. The velocity with the discretized pitch-rate concept is the highest and is 7.812 km/sec. This velocity is decreased to 7.808 km/sec when the continuous pitch-rate control variable smoothes out the discretized profile. However, in both the cases we have a discontinuity at the initial time. When this is removed by using pitching moment as the control variable, the final velocity is 7.783 km/sec, showing a reduction of about 30 m/sec. These results show that the inclusion of the rotational dynamics can be important in the study of trajectory optimization. This formulation removes various kinds of discontinuities present in the other formulations, and shows a reduction in the final performance. An ideal control system is used in this formulation. This can be modified to include the control system delays and other realistic factors.

References

[1] Spurlock, O.F. and Zarett, H., "Optimal Launch Trajectories for the ATS-E Mission," *Journal of Spacecraft and Rockets,* Vol. 8, Dec. 1971, pp. 1202-1208.

[2] Kelly, H.J., Uzzell, B.R. and McKay, S.S., "Rocket Trajectory Optimization by a Second-Order Numerical Technique," *AIAA Journal,* Vol. 7, May 1969, pp. 879-883.

[3] Rosenbaum, R., "A Combination of Numerical-Analytical Approach to Ascent Trajectory Optimization," AAS Science and Technology Series, Vol. 11, American Astronautical Society, Washington, D.C., 1967, pp. 243-262.

[4] Leondes, C.T. and Wu, C.A., "The Conjugate Gradient Method and its Application to Aerospace Vehicle Guidance and Control-I. Basic Results in Conjugate Gradient Method," *Astronautica Acta,* Vol. 17, Dec. 1972, pp. 871-880.

[5] Adimurthy, V. and Joy, K.V., "Trajectory Optimization of SLV-3" SSTC-ARD-TR-71-75, Jan. 1975, Space Science and Technology Centre, Trivandrum, India.

Shock Interference Peak Heating Measurements using Phase Change Coatings

J. Wayne Keyes*
NASA Langley Research Center, Hampton, Va.

Nomenclature

h	= heat transfer coefficient
M	= Mach number
n	= exponent, Eq. (1)
p	= pressure
PC	= phase change coating data, Fig. 3.
R	= Reynolds number
t	= time
T	= temperature
TC	= thermocouple data, Fig. 3
θ_{SL}	= shear-layer angle relative to local surface inclination

Subscripts

p	= peak
pc	= phase change
s	= stagnation
t	= total
w	= wall
$1,2,3,$ $4,5$	= regions of flowfield, Fig. 1

Introduction

THE phase change coating technique[1] has been used to obtain peak heating measurements in shock interference flow regions with high surface shear and heating.[2-4] This technique provides heat transfer coefficients which are determined by measuring the time for a point on the surface to reach the phase change temperature of the thin fusible coating. These values of time and temperature are then used with the solution to the transient one-dimensional heat conduction equation by assuming a step increase in heat input to ascertain the heat transfer coefficient. Motion picture photography is used to record the phase change pattern, and a precision clock is used to record the time required for the phase change to occur.

The purpose of this Note is to discuss some of the problems encountered in applying the phase change coating technique and to present new shock interference peak heating data which illustrates these problems. A 5.08-cm diameter hemisphere-cylinder made of silica based epoxy was tested at Mach 6 for freestream Reynolds numbers of 3.3 to 25.6 million per meter. Flat plate shock generator angles varied from 5° to 25°. A sketch of the shock interference pattern is shown in Fig. 1. This shock pattern consists of a plane shock intersecting the curved bow shock of the hemisphere thus creating a shear layer (type III interaction, Ref. 3) which attaches to or interacts with the hemisphere boundary layer causing high local pressure and heat transfer. Heating data obtained on a 5.08-cm diameter thin wall stainless steel hemispherical model instrumented with thermocouples every 5 deg on the vertical center line is also presented for the purpose of comparing the phase change technique with the thermocouple-calorimeter method.

Received July 21, 1975; revision received September 23, 1975.

Index categories: Boundary Layers and Convective Heat Transfer-Turbulent; Jets Wakes, and Viscid-Inviscid Flow Interactions; Supersonic and Hypersonic Flow.

*Aerospace Engineer, Applied Fluid Mechanics Section, High-Speed Aerodynamic Division.

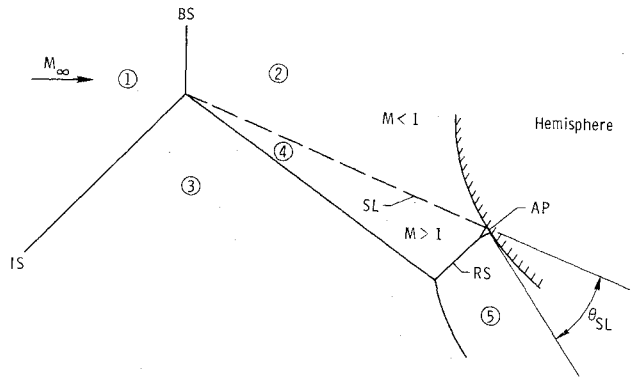

Fig. 1 Sketch of shear-layer flowfield. AP-attachment point; BS-bow shock; IS-impinging shock; RS-reflected shock; SL-shear layer.

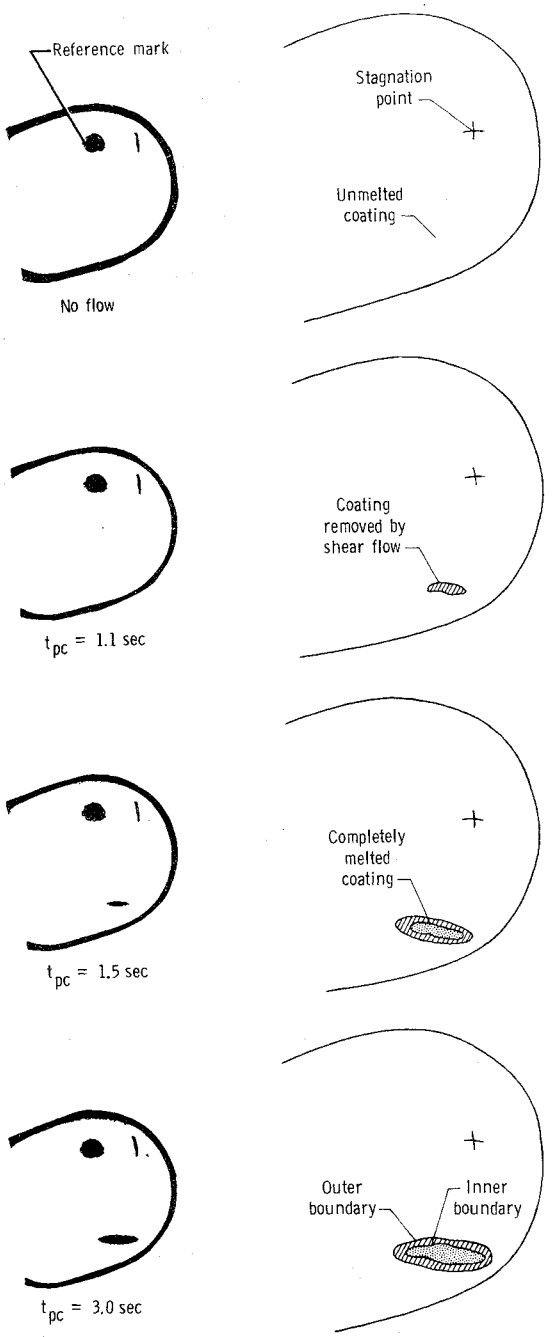

Fig. 2 Photographs and tracings of phase change patterns. T_{pc} = 422K, T_i = 297K, $T_{t,\infty}$ = 481K.

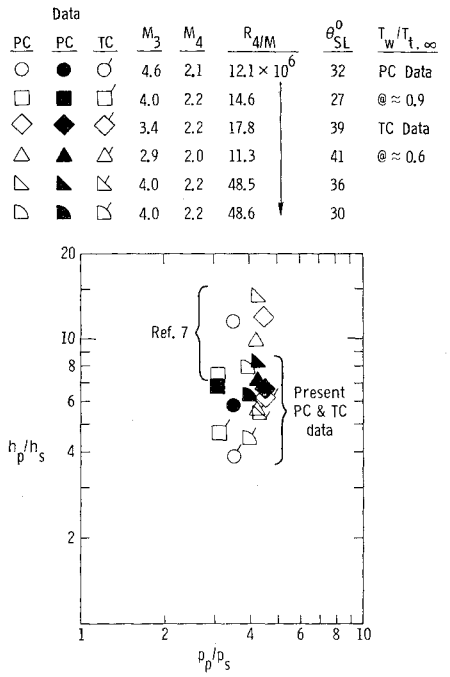

Fig. 3 Comparison of heating peaks.

Results and Discussion

Typical photographs and tracings of the present phase change patterns for shear-layer attachment on a hemisphere are shown in Fig. 2. The tracings are included to show the details of the melt region that would otherwise be lost in the reproduction of the photographs. When the model was first exposed to the flow, a dark area (cross-hatched area on tracing, $t_{pc} = 1.1$ sec.) appeared on the lower part of the model and possibly implies that melt has taken place. Careful examination of this and repeat tests showed that part of the coating was blown off by the high shear in the region of the attaching shear layer and, in fact, the coating had not melted. True melt was observed when an area of completely melted coating (black area) surrounded by a band of partially removed coating has formed on the lower surface (See Fig. 2, $t_{pc} = 1.5$ sec.). Therefore, peak heating was judged to occur where the black area first appeared on the model surface, and the inner boundary was thereafter taken as the line of constant heat transfer coefficient h (Fig. 2).

A comparison of the present maximum heating values from the phase change technique with those of Ref. 3 (which were obtained using the same model and in the same tunnel as for the present data) are shown in Fig. 3. These values are plotted in nondimensional form, h_p/h_s against p_p/p_s, since generally $h_p/h_s \propto (p_p/p_s)^n$ (Eq. 1) as suggested in Ref. 4. Stagnation values of h_s were calculated[3] and p_s values were measured directly. The difference between the two sets of phase change (*PC*) data for a given pressure ratio (open and filled symbols) is the result of a misinterpretation of when and where the phase change occurs. It was observed in the present investigation that a double phase change boundary occurs in the vicinity of shear-layer attachment as shown in Fig. 2. Only the outer boundary was observed in the investigation reported in Ref. 3 because of camera placement, camera setting, and/or lighting location. Using this outer boundary as the melt line resulted in higher heating rates (shorter melt times). In the present investigation the camera was positioned so that a better frontal view of the model and melt region was obtained. By using the inner boundary as the melt line as discussed previously, substantially lower heating values were obtained (closed symbols in Fig. 3).

Peak heating data (flagged symbols) measured with thermocouples on the thin skin model at the same pressure ratio as

the phase change data are shown in Fig. 3 for comparison with the phase change data. Thermocouple data are of course influenced by lateral conduction errors (15 to 20% for this case) and by errors due to peak heating not occurring exactly at a thermocouple location; however, the peak heating values from the thermocouple data as shown in Fig. 3 are not expected to be more than 30% low. The thermocouple data fall somewhat below the present *PC* data but are in substantially better agreement with the present *PC* data than that of Ref. 3.

These results show that quantitative peak heating data such as those caused by interfering flowfields can be measured using the phase change coating technique; this method also gives a more exact location of the peak. Caution should be used, however, when measuring high peaks resulting from high shear flows which might remove part or all of the coating and thus give a false impression of complete phase change. In addition, camera and lighting should be positioned so that the viewing angle is nearly normal to the melt surface.

References

[1] Jones, R.A. and Hunt, J.L., "Use of Fusible Temperature Indicators for Obtaining Quantitative Aerodynamic Heat-Transfer Data," NASA TR-R-230, 1966.

[2] Jones, R.A. and Hunt, J.L., "Measurements of Mutual Interference Heating for a Probe Antenna Mounted on an Apollo Reentry Configuration," NASA TM X-1787, 1969.

[3] Keyes, J.W. and Hains, F.D., "Analytical and Experimental Studies of Shock Interference Heating in Hypersonic Flow," NASA TN D-7139, 1973.

[4] Keyes, J.W. and Morris, D.J., "Correlations of Peak Heating in Shock Interference Regions at Hypersonic Speeds," *Journal of Spacecraft and Rockets*, Vol. 9, Aug. 1972, pp. 621-623.

Correction Factor for Heat Flux in an Expansion Nozzle

J. Reinkenhof* and R. Schmucker†
DFVLR, Lampoldshausen, West Germany

Introduction

WHEN calculating the local heat flux in a rocket-engine nozzle wall, a linear temperature distribution perpendicular to the wall surface is generally assumed.[1,2] This assumption is fully true only for a steady one-dimensional heat flow in a conductor with a temperature-independent thermal conductivity. This Note shows under what conditions the assumption of a linear temperature distribution will result in substantial errors. A correction factor is given to account for nonlinear temperature distribution.

Analysis

The expansion nozzle has the contour $y(x)$ on the hot-gas side, where x is the axis of rotation of the nozzle. The wall is assumed to be made of a material with a temperature-dependent thermal conductivity $\lambda\ (T)$. Figure 1 shows a curved wall element at point x. The nozzle contour is described by inclination angle ψ, defined as

$$\psi = \arctan\ |dy/dx| \tag{1}$$

The radius of curvature r of the nozzle contour is derived from

$$r = [1 + (dy/dx)^2]^{3/2} (d^2y/dx^2)^{-1} \tag{2}$$

where $r > 0$, if the concave side of the nozzle contour points to the positive direction of the curve normal. Using arc differential db, the heat-flow area in the element becomes

$$dA(z) = 2\pi(y + z\cos\psi)\ \frac{(r-z)}{r}\ db \tag{3}$$

If a linear temperature distribution $T(z)$ is assumed, the heat flux on the coolant side of the nozzle wall results from

$$q_{\text{lin}} = \lambda(T_{cw})\ \frac{T_{gw} - T_{cw}}{s} \tag{4}$$

T_{gw} being the hot-gas side wall temperature, T_{cw} that on the coolant side, and s the wall thickness. By using correction factor C, the real heat flux on the coolant side is determined by

$$q = C\ q_{\text{lin}} \tag{5}$$

The heat-balance of the element may be written as

$$-dA(z)\lambda(T)\ \frac{dT}{dz} = q[dA(z)]_{z=s} \tag{6}$$

because temperature gradients perpendicular to z are negligible, especially in the throat area.[3] Combining Eqs. (3-6) results in

$$\int_{T_{gw}}^{T_{cw}} \lambda(T)\,dT = -C\lambda(T_{cw})\,(T_{gw} - T_{cw})\,(y + s\cos\psi) \times \frac{(r-s)}{s} \int_0^s \frac{dz}{(r-z)\,(y + z\cos\psi)} \tag{7}$$

Finally, dimensionless variables are introduced

$$Y = y/y_t \tag{8a}$$

$$R = r/y_t \tag{8b}$$

$$S = s/y_t \tag{8c}$$

where y_t is the radius of the nozzle throat. The influence of temperature on λ is given by the dimensionless parameter

$$m = \lambda(T_{gw})/\lambda(T_{kw}) \tag{9}$$

If $\lambda\ (T)$ in Eq. (7) is replaced by a linear function and Eqs. (8)

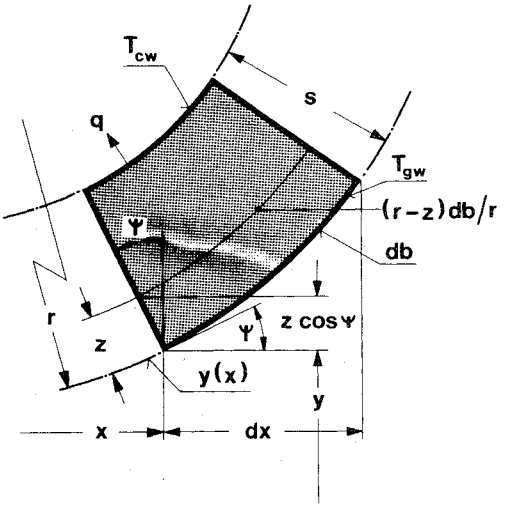

Fig. 1 Curved wall element for considering the heat balance.

Received August 29, 1975.
Index categories: Heat Conduction; Liquid Rocket Engines; Nozzle and Channel Flow.

*Scientist, Institut fuer Chemische Raketenantriebe.
†Head of the Research Division, Institut fuer Chemische Raketenantriebe. Associate Professor, Technical University of Munich. Member AIAA.